Computational manufacturing as a tool for the selection of the most manufacturable design

Tatiana V. Amotchkina,[1,3,4,*] Sebastian Schlichting,[2] Henrik Ehlers,[2] Michael K. Trubetskov,[1,3] Alexander V. Tikhonravov,[1] and Detlev Ristau[2,4]

[1]Research Computing Center, Moscow State University, Leninskie Gory, Moscow 119991, Russia

[2]Laser Zentrum Hannover e. V., Hollerithallee, 8, Hannover D-30419, Germany

[3]Max Planck Institute of Quantum Optics, Hans-Kopfermann strasse 1, Garching D-85748, Germany

[4]QUEST—Centre for Quantum Engineering and Space-Time Research, Welfengarten 1, Hannover D-30167, Germany

*Corresponding author: tatiana@srcc.msu.ru

Received 4 October 2012; revised 21 November 2012; accepted 21 November 2012; posted 21 November 2012 (Doc. ID 177466); published 17 December 2012

Applications of computational manufacturing experiments (CMEs) for selection of the most manufacturable designs among a variety of different design solutions are demonstrated. We compare design solutions with respect to estimations of their production yields. Computational experiments are performed using two simulation software tools. In the course of CMEs, we take into account all major factors causing errors in our deposition process. Real deposition experiments are in agreement with CMEs; the most manufacturable design exhibits better target performances compared to other designs.

OCIS codes: 310.1860, 310.4165, 310.3840, 310.6860.

1. Introduction

Today, multilayer optical coatings with complex wide-band spectral characteristics can be easily designed [1–5]. Moreover, modern design algorithms allow one to obtain multiple solutions of design problems. These design solutions exhibit excellent spectral performances and possess close combinations of the main design parameters [merit function (MF) value, number of layers N, total optical thickness (TOT)] [6–9]. These design solutions, however, reveal different sensitivity to deposition errors. It should be noted here that the stability of the design solutions is tightly interconnected with a monitoring technique used in the course of design deposition [10–12]. In the current work we deal with broadband optical monitoring systems performing thickness control in the course of the deposition process [13]. Among multiple designs, some solutions may be unstable even to small errors and cause failures in the deposition process. One of the main reasons for this instability is a cumulative effect [14]. For other designs, only a part of deposition runs are successful. At the same time, designs stable to deposition errors can be found.

As a quantitative measure of design stability to deposition errors, an estimation of production yield can be considered [10,11,15–18]. Deposition errors result in deviations of the coating performance from the performance of the corresponding theoretical design. Typically, to distinguish between successful and unsuccessful deposition runs, allowed corridors of deviations from target spectral characteristics are specified. Samples with spectral characteristics lying inside such corridors are considered as successful ones [10,11,15,16,19]. Evidently, performing a representative number of real deposition runs is quite expensive and time consuming. In recent years, computational manufacturing experiments (CMEs)

1559-128X/12/368677-10$15.00/0

simulating real deposition runs have been intensively used for design selection [10,17,18,20–22].

In the case of nonoptical monitoring techniques (time control and quartz crystal monitoring), CMEs are based on standard Monte Carlo statistical tests with randomly distributed thickness errors or/and deviations in refractive indices. In the case of optical monitoring techniques, CMEs are performed with the help of specially elaborated software tools [17,20,21,23–26]. In our recent publication [27], we proposed to include computational manufacturing into modern design-production chains for multilayer coatings, as is sketched in Fig. 1. Selection of the most manufacturable designs with the help of CME is shown in Fig. 1 (left dot-dashed rectangle).

Evidently, estimations of design production yields can be considered as reliable ones only if simulations of real deposition runs are performed with adequate model simulation parameters. For example, in [17] a series of single-layer samples were produced in order to investigate the reproducibility of layer properties and specify deposition errors in the course of simulations. In our previous work [27] we proposed an approach that allows one to establish relevant relations between simulations and deposition processes (see right dashed rectangle in Fig. 1). This approach is based on CME, and it has been realized for the case of the broad-band monitoring (BBM) technique.

In our present study it is demonstrated how CME can be used for selection of the most manufacturable design, i.e., a design providing the highest production yield in the case of using a particular monitoring technique. We shall concentrate on the BBM technique. It should be noted here that in our paper a real practical problem of edge filters (EFs) design is considered. We perform CME using two different simulation software tools: a BBM simulator developed at Laser Zentrum Hannover (BBM LZH) [20,24] and a BBM simulator incorporated into OptiLayer thin film software (BBM OL) [22,23,28].

In Section 2, we present our design problem, describe synthesis algorithms, and obtain 10 design solutions. In Section 3, we perform multiple CMEs using BBM OL and find two of the most stable and two of the most unstable designs. In Section 4, we provide results of the CME obtained using BBM LZH and finally select four designs: two with the highest production yield and two with a low production yield. In Section 5, we deposit both designs and report about our experimental results. Final conclusions are presented in Section 6.

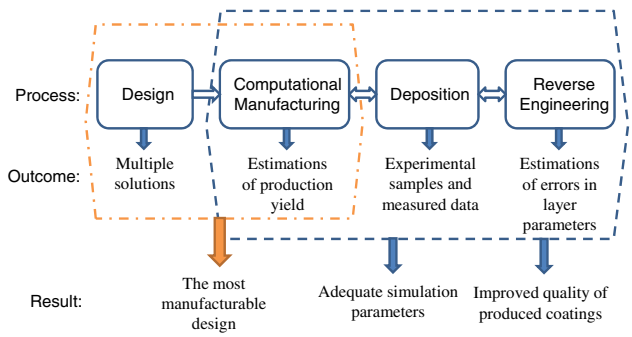

Fig. 1. (Color online) Schematic representation of modern design-production chain.

2. Design Problem and Design Solutions

In order to demonstrate our approach to design selection, we consider a design problem of EFs. The target transmittance is 100% in the spectral range from 670 to 710 nm, and the target reflectance is 100% in the spectral range from 585 to 643 nm; the angle of incidence (AOI) is 45°, and light is unpolarized. In the design process, we use titanium dioxide as a high-index material and silicon dioxide as a low-index material. Refractive indices $n_H(\lambda)$, $n_L(\lambda)$ of these materials are specified by Sellmeier equations:

$$n^2(\lambda) = 1 + \frac{A_1\lambda^2}{\lambda^2 - A_2} + \frac{A_3\lambda^2}{\lambda^2 - A_4}, \quad (1)$$

where $A_1 = 4.062, A_2 = 0.048857, A_3 = 1.40166$, and $A_4 = 80$ for TiO_2 and $A_1 = 1.158586, A_2 = 0.010727$, $A_3 = 0.5$, and $A_4 = 61$ for SiO_2; λ in this formula should be expressed in micrometers. Extinction coefficient $k(\lambda)$ of TiO_2 is estimated as $k(400) = 0.0036$, $k(450) = 0.0015$, $k(500) = 0.0006$, $k(550) = 0.0003$, $k(600) = 0.0001$, and $k(\lambda) = 0$ for $\lambda > 600$ nm. These optical constants were determined in our previous paper [27] in the course of establishing proper relations between simulation and deposition processes. In what follows we shall refer to these indices as *nominal* ones. The substrate is Suprasil of 1 mm thickness.

In order to obtain design solutions, we use numerical algorithms incorporated into OptiLayer thin-film software [2,3,6,23]. Different designs can be obtained using a combination of random optimization and needle optimization algorithms. The random optimization algorithm is useful for solving complicated design problems when good starting designs are unknown [9]. The algorithm generates a sequence of starting designs with the indicated number of layers and layer thicknesses that are uniformly distributed random numbers with specified average values. Each design is optimized by an efficient method, such as the Newton method, the modified damped least-squares, or the sequential quadratic programming method. The obtained designs are used as starting designs for the needle optimization algorithm [3]. In order to exclude thin layers from the designs obtained by the needle optimization algorithm, a special procedure, removing thin layers within the limits of an acceptable increase of the MF value, is applied [3].

In order to estimate the closeness between the target and actual design spectral characteristics, we introduced a MF in a standard way [29]:

$$\mathrm{MF} = \left\{ \frac{1}{3L_1} \sum_{k=1}^{3} \sum_{j=1}^{L_1} [R(\lambda_j, \theta_k) - 100\%]^2 + \frac{1}{3L_2} \sum_{k=1}^{3} \sum_{j=1}^{L_2} [T(\lambda_j, \theta_k) - 100\%]^2 \right\}^{1/2}, \quad (2)$$

where $\{\lambda_j\}$ is the wavelength grid with 1 nm step specified in the range $[585, 643]$ nm ($L_1 = 61$ spectral points) in the first term and in the range $[670, 710]$ nm ($L_2 = 41$ spectral points) in the second term. In Eq. (2), θ_k are AOI equal to 43°, 45°, and 47°. Although the target specifications are formulated only for AOI = 45°, we reserved a wider AOI range with ±2° extend for better manufacturability of coatings.

Structures of 10 design solutions EF1–EF10 are presented in Tables 1 and 2. Principle design parameters of these solutions are shown in Table 3. It is seen that all solutions contain 27–30 layers and have close values of TOT and MF. MF values achieved with all designs are smaller than one, which can be interpreted as less than 1% deviations between target and design spectral characteristics.

Table 1. Structures of the Design Solutions EF1–EF5

Layer Number	Physical Thickness (nm)					Material
	EF1	EF2	EF3	EF4	EF5	
1	36.24	60.09	65.25	41.37	80.21	TiO_2
2	153.83	290.72	288.59	137.35	308.90	SiO_2
3	154.98	72.09	73.36	160.27	28.74	TiO_2
4	156.98	135.66	128.54	142.52	163.59	SiO_2
5	72.17	78.23	79.28	73.82	73.42	TiO_2
6	95.23	288.88	286.67	115.32	128.62	SiO_2
7	87.03	75.06	85.32	102.03	93.44	TiO_2
8	540.78	163.93	146.30	78.89	247.76	SiO_2
9	80.17	162.80	168.60	166.74	85.83	TiO_2
10	126.78	154.93	146.08	131.41	126.30	SiO_2
11	206.83	79.64	78.99	83.53	72.16	TiO_2
12	130.90	338.21	345.50	116.44	126.07	SiO_2
13	84.93	90.48	85.95	73.16	78.09	TiO_2
14	263.24	271.75	275.82	138.55	218.22	SiO_2
15	84.56	84.37	86.84	310.11	121.98	TiO_2
16	128.30	132.24	123.60	136.29	129.54	SiO_2
17	71.90	72.42	75.46	71.01	73.15	TiO_2
18	126.86	155.07	146.19	123.27	128.49	SiO_2
19	79.18	303.13	308.24	80.60	76.70	TiO_2
20	228.91	153.22	153.03	147.43	158.93	SiO_2
21	121.10	74.82	74.62	145.64	137.15	TiO_2
22	132.80	95.65	100.04	150.70	164.63	SiO_2
23	76.52	50.93	52.90	82.92	78.51	TiO_2
24	107.75	350.02	352.45	124.35	124.02	SiO_2
25	46.38	78.66	69.79	82.25	62.80	TiO_2
26	92.29	84.63	95.60	51.03	582.08	SiO_2
27	78.00	30.00	30.00	63.46	57.77	TiO_2
28	351.75			361.02	196.09	SiO_2
29	30.00			50.02		TiO_2
30				209.34		SiO_2
	1309.99	1312.72	1334.6	1586.93	1119.95	$\sum TiO_2$
	2636.4	2614.91	2588.41	2163.91	2803.24	$\sum SiO_2$

In order to distinguish between successful and unsuccessful deposition runs, we specify range targets. Reflectance should be more than 99% in the spectral range from 585 to 635 nm and more than 89% at $\lambda = 643$ nm. Transmittance should be more than 93.5% in the spectral range from 670 to 710 nm. Range target values were specified in the case when substrate back-side reflections are taken into account.

3. Estimation of Production Yields Based on OptiLayer Simulator

First, we use BBM OL to investigate the stability of the obtained design solutions with respect to deposition errors and to estimate production yields. Due to the very fast algorithms incorporated in this simulator, hundreds of CMEs can be performed in a very short time.

The BBM OL simulation algorithm models most of the factors causing production errors in a typical deposition chamber:

- Mean deposition rates of high- and low-index materials r_H and r_L and their fluctuations, δr_H and δr_L, are specified. Dependencies of deposition rates on time are modeled as stationary random processes with correlation times, τ_H and τ_L, of several seconds.

Table 2. Structures of the Design Solutions EF6–EF10

Layer Number	Physical Thickness (nm)					Material
	EF6	EF7	EF8	EF9	EF10	
1	35.76	189.01	30.28	16.73	197.05	TiO_2
2	328.71	314.64	113.17	85.88	574.47	SiO_2
3	76.77	74.08	331.66	792.12	69.22	TiO_2
4	148.92	139.71	134.81	120.18	128.20	SiO_2
5	148.27	188.73	49.78	781.71	87.80	TiO_2
6	183.21	324.15	152.89	112.88	269.27	SiO_2
7	65.37	78.93	221.60	69.98	90.14	TiO_2
8	129.17	134.90	30.00	128.46	154.17	SiO_2
9	62.05	87.48	209.89	327.67	166.71	TiO_2
10	184.69	270.27	149.61	113.04	156.17	SiO_2
11	143.69	92.30	85.03	71.54	74.44	TiO_2
12	142.65	144.39	65.19	81.16	85.55	SiO_2
13	70.99	172.38	90.42	80.69	104.56	TiO_2
14	131.11	139.39	135.76	134.72	262.52	SiO_2
15	74.27	76.85	166.59	321.44	82.01	TiO_2
16	162.18	154.46	95.65	134.44	130.13	SiO_2
17	148.01	152.11	87.27	70.34	82.82	TiO_2
18	165.32	156.86	116.63	101.29	321.81	SiO_2
19	202.96	76.44	71.48	52.87	212.27	TiO_2
20	141.01	149.57	156.90	106.58	117.53	SiO_2
21	79.36	163.40	306.82	332.44	206.71	SiO_2
22	298.99	155.08	149.00		87.62	TiO_2
23	78.14	70.33	70.96		48.52	TiO_2
24	145.36	122.78	107.87		210.84	SiO_2
25	29.96	33.82	43.40			TiO_2
26	144.87	102.97	119.09			SiO_2
27	45.99	58.05	208.91			TiO_2
28	113.66	209.38	99.81			SiO_2
29	29.96		30.28			TiO_2
	1291.52	1513.90	2004.37	2917.53	1422.24	$\sum TiO_2$
	2419.84	2518.56	1626.38	1118.65	2498.29	$\sum SiO_2$

Table 3. Principle Parameters of the Obtained Design Solutions

Deposition	Number of Layers	TOT at $\lambda = 750$ nm	Merit Function
EF1	29	3946.4	0.43
EF2	27	3927.6	0.85
EF3	27	3923.0	0.47
EF4	30	3750.8	0.29
EF5	28	3923.2	0.55
EF6	29	3711.4	0.47
EF7	28	4032.5	0.61
EF8	29	3630.8	0.46
EF9	21	4036.2	0.73
EF10	24	3920.5	0.77

Details of deposition rates modeling can be found in [22]. In our CME we specify $r_H = 0.3$ nm/s, $r_L = 0.55$ nm/s, $\delta r_H = 0.03 r_H$, $\delta r_L = 0.12 r_L$, $\tau_H = 15$ s, and $\tau_L = 1$ s. These values are quite close to real deposition parameters.

- Systematic and random deviations of optical constants of layer materials from their nominal values as well as the level of systematic inhomogeneities of the design layers may be specified. These simulation parameters are described in detail below.
- Typical parameters of a monitoring system are specified. Namely, these parameters are the type of spectral photometric data (R or T), AOI, time interval between on-line data scans Δt, shutter delays Δs and their rms deviations $\delta\Delta s$, boundaries of the broadband spectral range, λ_l, λ_u, and a number of wavelength points in this range L. In our study, we take $\Delta t = 2$ s and $\Delta s = 0.35$ s, $\delta\Delta s = 0.08$ s, $\lambda_l = 420$ nm, $\lambda_u = 950$ nm, and AOI = 4°.
- Signal errors are specified as a random noise with the level δT added to every measurement data scan. In order to simulate calibration drifts and instabilities, additional systematic offsets are added. Similarly to deposition rates, these offsets are represented as a stationary random process with fluctuations ΔT and correlation time τ_S. In our study we take $\delta T = 1\%$, $\Delta T = 0.15\%$, and $\tau_S = 5$ s.

In the course of CME, successive on-line transmittance data scans are analyzed by the incorporated control algorithm in order to determine termination points for layer depositions [30]. These points are calculated on the basis of thickness values estimated by the on-line characterization algorithm. This algorithm is minimizing a discrepancy function:

$$\mathrm{DF}(d(t)) = \left(\frac{1}{L}\sum_{j=1}^{L}[T(d_1,\ldots,d_{i-1},d(t),\lambda_j) - \hat{T}(\lambda_j)]^2\right)^{1/2} \tag{3}$$

with respect to the thickness of the current layer d with the number i. In Eq. (3), $\hat{T}(\lambda_j)$ is the current data scan, and $d_1,\ldots,d_{i-1}$ are estimated layer thicknesses.

It has been known that possible deviations of refractive indices and extinction coefficients strongly affect the monitoring procedure [27,31,32]. Therefore realistic simulation of the deposition process requires introduction of optical-constant deviations along with other simulation parameters listed above. For example, in [17] optical constants were described using the Lorentz dispersion model, and the model parameters were varied using Gaussian distribution with known mean value and standard deviation obtained as results of a special series of experiments.

In our present study we compare nominal refractive indices of TiO_2 and SiO_2 and refractive indices obtained as results of the reverse-engineering procedure performed after multiple deposition test experiments at the same deposition plant (Fig. 2) and find that absolute deviations between nominal refractive indices and refractive indices determined by the reverse-engineering procedure do not exceed 0.015 for TiO_2 and 0.01 for SiO_2. We specify the levels of these deviations in the course of CME. It is also possible that optical constants of layer materials can vary from layer to layer due to slow changes in various factors affecting the deposition process inside the vacuum chamber.

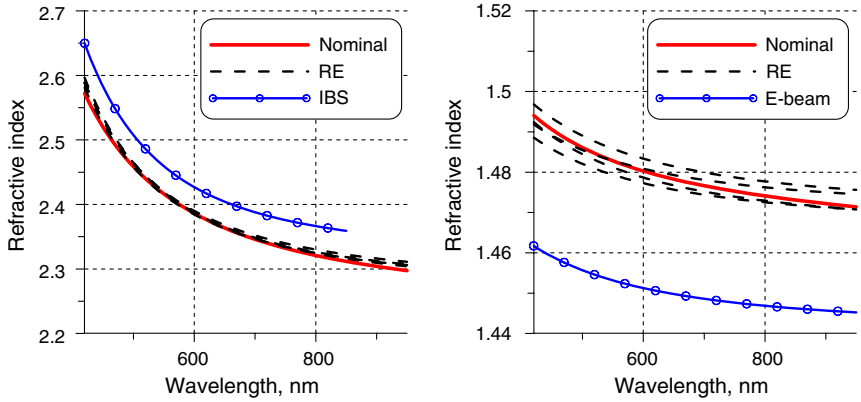

Fig. 2. (Color online) Nominal refractive indices of TiO_2 (left side) and SiO_2 (right side). Dashed curves indicate refractive indices of TiO_2 and SiO_2 determined in the course of a reverse engineering (RE) procedure from experimental data related to four produced test coatings [27]. Marked curves show the refractive index of TiO_2 film produced by IBS [33] and the refractive index of SiO_2 film produced by e-beam evaporation [34].

We assume also that dispersion behavior of TiO_2 and SiO_2 optical constants was found correctly because these dependencies are consistent with the dependencies determined earlier. For comparison, in Fig. 2 we present the refractive index of TiO_2 single layer produced by ion-beam sputtering (IBS) [33] and the refractive index of SiO_2 single layer produced by *e*-beam evaporation [34].

Taking into account the reasons mentioned above, in the course of CME we specify only offsets, Δn_H, Δn_L, of TiO_2 and SiO_2 refractive indices and do not vary the shape of their dispersion curves. This means that simulated measurement data $\hat{T}(\lambda_j)$ are calculated with refractive indices $n_H(\lambda) + \Delta n_H$, $n_L(\lambda) + \Delta n_L$ instead of $n_H(\lambda)$, $n_L(\lambda)$. Assuming that dispersion curves can be shifted upward or downward, we perform four series of CME for each EF design. Namely, we specify systematic offsets in refractive indices ± 0.015 for TiO_2 and ± 0.01 for SiO_2. Four combinations are to be considered: $\Delta n_H = 0.015$, $\Delta n_L = 0.01$; $\Delta n_H = 0.015$, $\Delta n_L = -0.01$; $\Delta n_H = -0.015$, $\Delta n_L = 0.01$; and $\Delta n_H = -0.015$, $\Delta n_L = -0.01$.

In [10] we proved that generally, for confident estimation of production yield Y, a large number of CMEs should be performed. For example, achieving 95% confidence level of estimation requires at least 2700 CME. Probability theory predicts that the poorest accuracy of production yield estimations corresponds to intermediate Y values from 20% to 80%. The goal of the present study is not to estimate production yields with a high accuracy but to estimate a production yield with an accuracy that would allow us to distinguish between stable and unstable design solutions. Therefore, in our case, if a rough estimation of the production yield is not high enough, then it is not reasonable to estimate it with a higher accuracy. If we observe that in a series of CMEs with a chosen design, after 10–20 simulation runs, production-yield estimation Y is less than 60%–80%, we consider this design as an unstable one in this series of CMEs. On the contrary, we need more accurate estimations for production yields of those designs that provide values close to 100%. Fortunately, the theory predicts much better accuracy of estimations for such Y values than for intermediate Y values. For example, $Y = 100\%$ can be confirmed by 100 successful CMEs with confidence about 6%.

First, we perform 20 CMEs in each series listed above, and estimate corresponding production yields $Y_1, \ldots, Y_4$. Then, for designs with $Y_i > 90\%$, we perform an additional 100 CMEs in order to estimate high levels of production yields more accurately and reliably. The average yields $Y = (Y_1 + \ldots + Y_4)/4$ are collected in Table 4. It is seen that two designs, EF7 and EF8, show 100% yield. These design solutions can be considered as stable ones. Designs EF2, EF9, and EF10 show low yields and can be considered as unstable ones. Designs EF1 and EF3–EF6 exhibit intermediate yields and also can be rated as unstable.

Table 4. Production Yields Estimated with the Help of BBM OL

Design	Production Yield Y (%) BBM OL	BBM LZH
EF1	95	80
EF2	38	40
EF3	52	50
EF4	75	70
EF5	67	50
EF6	45	25
EF7	100	100
EF8	100	100
EF9	35	50
EF10	25	15

4. Investigation of the Design Manufacturability with BBM LZH Simulator

We perform a number of CMEs using BBM LZH for our 10 design solutions. This software tool allows us to make the final decision about design feasibility because the real-time BBM LZH algorithm will control deposition of layers. This algorithm is incorporated to the Leybold SYRUS Pro 1100 deposition plant and has been carefully tested on a large number of experimental runs [18,20,24]. BBM LZH models all major factors causing errors in the course of the deposition; the set of these factors is close to BBM OL. In our experiments, BBM LZH values of these factors were selected in close matching with BBM OL settings; the only differences are listed below:

- Offset of shutter delay 350 ± 80 ms was specified instead of shutter delays Δs and their rms deviations $\delta\Delta s$.
- Systematic deviations of optical constants of layer materials were specified as systematic offsets of Sellmeier formula coefficients as indicated below.

We perform four series of CMEs for each of designs EF1–EF10. In each series we perform 10 CMEs; in the cases when production yield is more than 80%–90%, we perform an additional 40 CMEs. In the series of CMEs, we specify the same variations of the layer refractive indices as we took in the course of CMEs with BBM OL. In the case of BBM LZH, it is more convenient to specify the systematic offsets of refractive indices in terms of Sellmeier coefficients. Namely, the offsets ± 0.015 for TiO_2 refractive index are described by variations in Sellmeier coefficients $\Delta A_1 = \pm 1.65\%$, $\Delta A_2 = -0.7\%$, and the offset ± 0.01 for SiO_2 index is achieved by variations $\Delta A_1 = \pm 2.5\%$, $\Delta A_2 = \mp 1.6\%$. For each design solution we find estimations of production yields $Y_1, \ldots, Y_4$ and calculate average yield $Y = (Y_1 + \ldots + Y_4)/4$.

Estimations of production yields Y are presented in Table 4. It is seen that designs EF7 and EF8 exhibit the maximal yields and can be considered as stable ones. Other designs provide low or intermediate yields and can be considered as unstable ones.

From Table 4 one can observe that design solutions EF7 and EF8 are the most stable according to

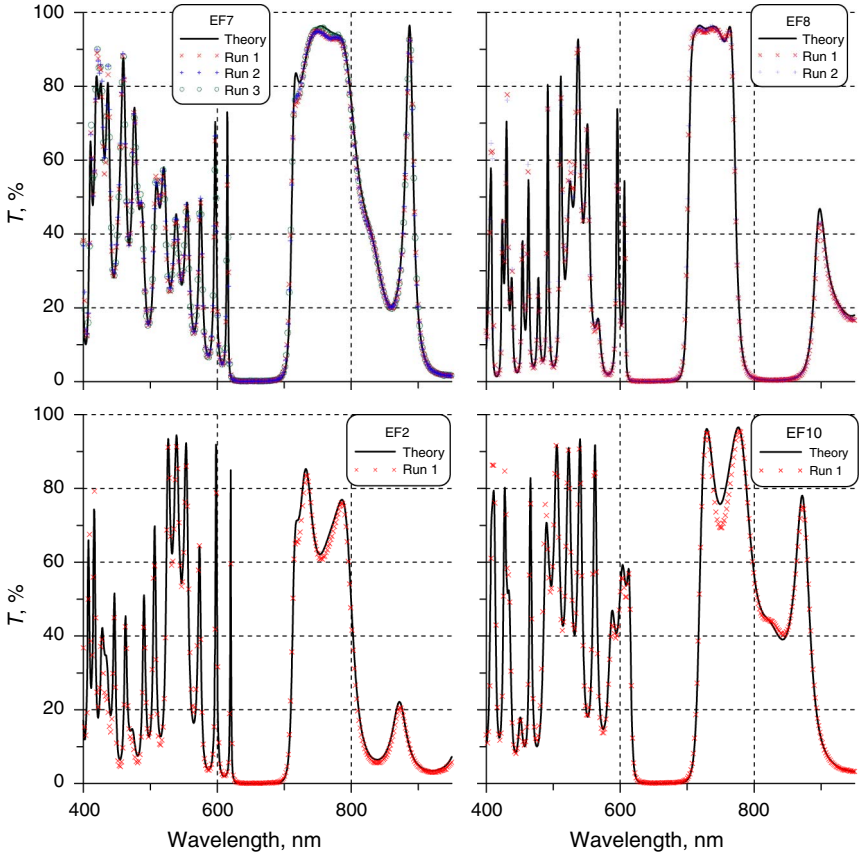

Fig. 3. (Color online) Comparison of theoretical (black curves) and experimental (crosses) normal-incidence transmittance data related to produced designs.

the estimations obtained with the help of both simulators. We can recommend these designs for practical realization. In order to check the reliability of our yield estimations, we need to also produce designs with low production yields. On the basis of CME results performed using BBM OL and BBM LZH, we select solutions EF2 and EF10 as unstable ones.

5. Experimental Results

We performed seven real deposition runs and produced seven samples: three samples of EF7 design, two samples of EF8 design, one sample of EF2 design, and one sample of EF10 design. The ion-assisted deposition process based on the Leybold SYRUSPro 1100 deposition plant equipped with an APSpro was used. In Fig. 3, theoretical and experimental normal incidence transmittance data of some of the deposited samples are compared. The correspondence between theoretical and experimental transmittances for the designs EF7 and EF8 is noticeably better than that for the designs EF2 and EF10.

As the target spectral characteristics and range targets are specified for oblique incidence, we

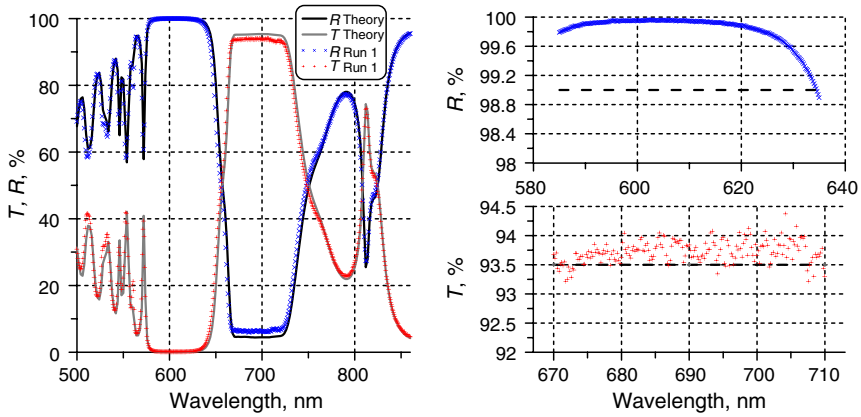

Fig. 4. (Color online) Sample EF7–Run1, AOI = 45°: comparison of theoretical reflectance and transmittance (black and gray curves) with experimental reflectance and transmittance (crosses). Dashed horizontal lines indicate range targets.

measured transmittance at AOI = 45° using Perkin Elmer Lambda 900. This device allows us to measure transmittances $\hat{T}^{(s)}(\lambda_j)$ and $\hat{T}^{(p)}(\lambda_j)$ for s- or p-polarized light, in the spectral range from 500 to 850 nm.

In the left sides of Figs. 4–7, we compare theoretical characteristics of designs EF7, EF8, EF2, and EF10 and experimental transmittance data related to some of produced samples. Theoretical reflectances and transmittances are calculated for unpolarized light, AOI = 45°, and substrate back side is taken into account. Experimental transmittance data $\hat{T}(\lambda_j)$ are calculated as $(\hat{T}^{(s)}(\lambda_j) + \hat{T}^{(p)}(\lambda_j))/2$. It can be easily calculated that deviation between theoretical reflectance of the EF designs with and without taking into account

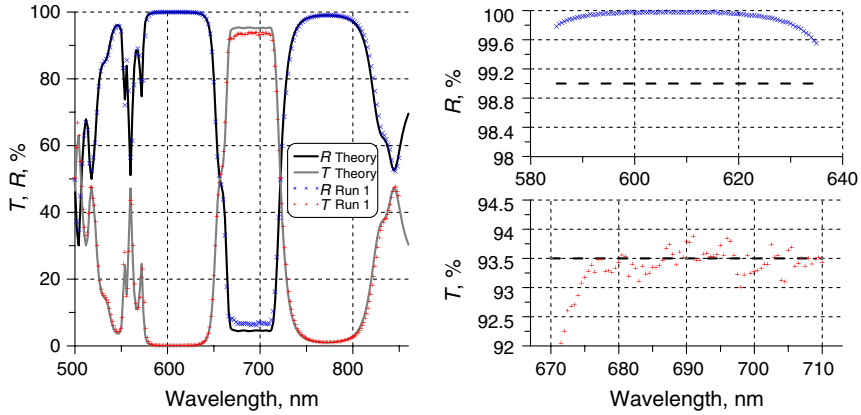

Fig. 5. (Color online) Sample EF8–Run1, AOI = 45°: comparison of theoretical reflectance and transmittance (black and gray curves) with experimental reflectance and transmittance (crosses). Dashed horizontal lines indicate range targets.

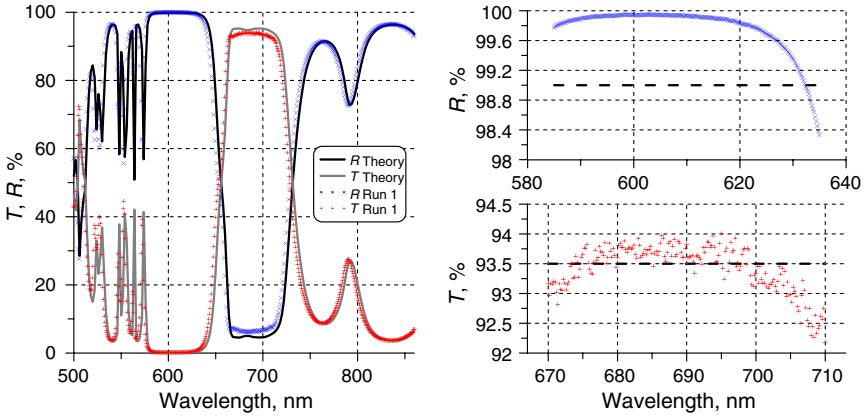

Fig. 6. (Color online) Sample EF2–Run1, AOI = 45°: comparison of theoretical reflectance and transmittance (black and gray curves) with experimental reflectance and transmittance (crosses). Dashed horizontal lines indicate range targets.

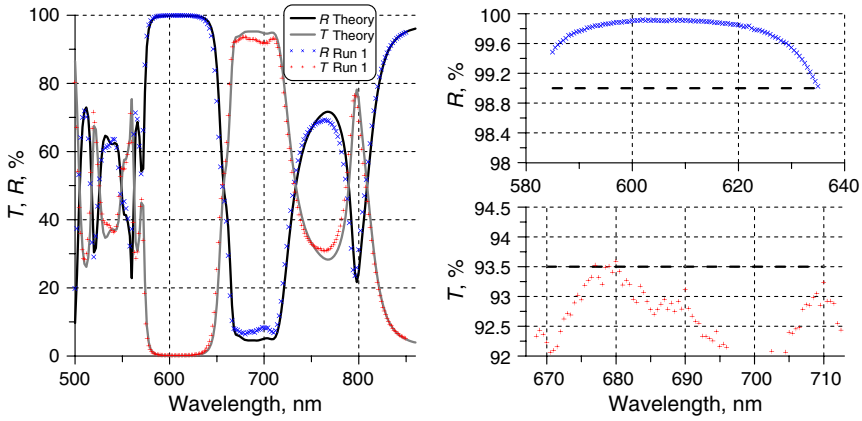

Fig. 7. (Color online) Sample EF10–Run1, AOI = 45°: comparison of theoretical reflectance and transmittance (black and gray curves) with experimental reflectance and transmittance (crosses). Dashed horizontal lines indicate range targets.

absorption of TiO_2 layers does not exceed 0.05% in the range from 580 to 643 nm. Also, the deviations between theoretical reflectance of the designs, calculated with a nominal extinction coefficient and doubled extinction coefficient, do not exceed 0.1% in the same range. These considerations are in a full agreement with the well-known fact that a slight absorption in layers affects the transmittance and almost does not affect the reflectance data. Based on these considerations, we can identify the experimental reflectance and reflectance $\hat{R}(\lambda_j)$ calculated from transmittance data as $100\% - \hat{T}(\lambda_j)$.

In the right sides of Figs. 4–7, we present the same experimental reflectance and transmittance values but in a larger scale in order to check whether they lie inside allowed corridors. It is seen from Fig. 4 that experimental data related to the EF7 sample are lying inside allowed corridors: $\hat{R}(\lambda_j) > 99\%$ in the range from 585 to 635 nm and $\hat{T}(\lambda_j) > 93.5\%$ in the range from 670 to 710 nm, respectively.

For experimental data related to the EF8 sample (Fig. 5), it is seen that transmittance data is outside of the allowed corridor $\hat{T}(\lambda_j) > 93.5\%$. Worse performance of design EF8 in comparison with performance of design EF7 can be explained by the fact that EF8 contains more TiO_2 (i.e., the total thickness of TiO_2 layers in EF8 is larger than the total thickness of TiO_2 layers in EF7), and errors in the extinction coefficient of TiO_2 may cause deviations between theoretical and experimental transmittance of the EF8 design.

It is seen from Fig. 6 that the reflectance of the EF2 sample is lower than the range target value for $\lambda > 632$ nm and that the transmittance is lower than 93.5% in many spectral points in the [670, 710] nm spectral range. These experimental results are in full agreement with our theoretical expectations based on the analysis of CME results.

As expected on the basis of CME results, spectral transmittance of the EF10 sample is outside of the allowed corridor in the [670, 710] nm range (see Fig. 7).

In order to numerically compare deviations of experimental spectral characteristics of the produced samples with their theoretical characteristics, we introduce a discrepancy function and a generalized discrepancy function. The discrepancy function estimates closeness between theoretical and measured transmittance of the samples:

$$\mathrm{DF}_0 = \left(\frac{1}{L}\sum_{j=1}^{L}[T(\lambda_j) - \hat{T}(\lambda_j)]^2\right)^{1/2}, \tag{4}$$

where $\{\lambda_j\}$ is the wavelength grid in the [420, 950] nm spectral range, $\hat{T}(\lambda_j)$ is the measured transmittance, and $T(\lambda_j)$ is the theoretical transmittance, respectively.

The generalized discrepancy function estimates closeness between theoretical and measured transmittance data taken after deposition of each layer [35,36]:

Table 5. Comparison of Discrepancy Values Calculated for Experimental Samples

Design Run	DF_0	GDF	DF^t
EF7–Run1	2.4	1.7	6.3
EF7–Run2	2.7	1.8	6.2
EF7–Run3	2.3	1.7	6.3
EF8–Run1	3.88	2.52	6.7
EF8–Run2	3.6	2.21	7.3
EF2	3.3	2.1	6.6
EF10	3.18	1.8	7.5

$$\mathrm{GDF} = \left(\frac{1}{NL}\sum_{k=1}^{N}\sum_{j=1}^{L}[T^{(k)}(\lambda_j) - \hat{T}^{(k)}(\lambda_j)]^2\right)^{1/2}, \tag{5}$$

where N is the number of layers in the design, and λ_j varies in the [420, 950] nm spectral range. The number of wavelength points in Eqs. (4) and (5) is $L = 1196$.

From a practical point of view, it may be useful to estimate numerically the closeness of experimental characteristics $\hat{T}(\lambda)$, $\hat{R}(\lambda)$ to target characteristics $T^{(t)}(\lambda)$, $R^{(t)}(\lambda)$. In order to do this, we consider a function

$$\mathrm{DF}^t = \left(\frac{1}{L_1}\sum_{\{\lambda_j\}_1}[\hat{R}(\lambda_j) - 100\%]^2 + \frac{1}{L_2}\sum_{\{\lambda_j\}_2}[\hat{T}(\lambda_j) - 100\%]^2\right)^{1/2}, \tag{6}$$

where $\{\lambda_j\}_1$ and $\{\lambda_j\}_2$ are the wavelength grids in the spectral ranges of [585, 635] nm (L_1 points) and [670, 710] nm (L_2 points), respectively.

We calculated discrepancies on the basis of measurement data related to the seven produced samples. These values are presented in Table 5. In this table one can observe that in general all discrepancies, DF_0, GDF, and DF^t are lower for EF7 samples (rows 2, 3, and 4) than discrepancies of all other samples. Design EF8 exhibits high production yield, but in the real experiments problems with obtained performance are revealed. As has been mentioned above, it can be explained by 30%–40% larger content of TiO_2 in the corresponding design, which can lead to more pronounced additional effects of inhomogeneities and/or absorption of thick TiO_2 layers not included to CME.

6. Conclusions

In our study, we demonstrated how CME can be used for the selection of feasible designs among a variety of different design solutions. In order to distinguish between stable and unstable designs, we used estimations of the production yields obtained by two different BBM simulators. We ranged our design solutions with respect to the estimations of production yields. In the course of CME we specified all major factors causing errors during the deposition process in accordance with preliminary studies of

the deposition process and monitoring system instabilities. The most critical factors are possible variations of layer optical constants. We carefully investigated the stability of simulated designs spectral characteristics with respect to different types of variations of refractive indices.

On the basis of a comparison of production-yield estimations obtained with two simulators, we selected four design solutions: two the most manufacturable ones and two unstable ones. We produced these designs and demonstrated that experimental results were in a full agreement with our theoretical expectations. The most manufacturable design samples exhibited better performances than the samples of the unstable ones. In our study we demonstrated that CME can be considered as a powerful numerical tool for selection of feasible design solutions.

This work was supported by the German Federal Ministry of Economics and Technology (research project TACo—Tailored Automated Coating, Contract No. 16IN0407), the DFG Cluster of Excellence, "Munich Centre for Advanced Photonics" (http://www.munich-photonics.de), the Russian Fund of Basic Research (project 10-07-00480-a and 11-07-91153a), and the Centre for Quantum Engineering and Space-Time Research (QUEST).

References

1. J. Kruschwitz, "Software tools speed optical thin-film design," Laser Focus World **39**, 157–166 (2003).
2. A. V. Tikhonravov, M. K. Trubetskov, and G. W. DeBell, "Application of the needle optimization technique to the design of optical coatings," Appl. Opt. **35**, 5493–5508 (1996).
3. A. V. Tikhonravov, M. K. Trubetskov, and G. W. DeBell, "Optical coating design approaches based on the needle optimization technique," Appl. Opt. **46**, 704–710 (2007).
4. V. Pervak, M. K. Trubetskov, and A. V. Tikhonravov, "Robust synthesis of dispersive mirrors," Opt. Express **19**, 2371–2380 (2011).
5. A. V. Tikhonravov and M. K. Trubetskov, "Modern design tools and a new paradigm in optical coating design," Appl. Opt. **51**, 7319–7332 (2012).
6. A. V. Tikhonravov, M. K. Trubetskov, T. V. Amotchkina, and M. A. Kokarev, "Key role of the coating total optical thickness in solving design problems," Proc. SPIE **5250**, 312–321 (2004).
7. A. Tikhonravov, M. Trubetskov, and I. Kasahara, "Achievements and challenges in the design and production of high quality optical coatings," IEICE Trans. Electron. **E91-C**, 1622–1629 (2008).
8. A. V. Tikhonravov and M. K. Trubetskov, "Design opportunities for better manufacturability," in *Optical Interference Coatings*, Technical Digest (CD) (Optical Society of America, 2011), p. WA2.
9. A. V. Tikhonravov and M. K. Trubetskov, "Modern status and prospects of the development of methods of designing multilayer optical coatings," J. Opt. Technol. **74**, 845–850 (2007).
10. A. V. Tikhonravov, M. K. Trubetskov, T. V. Amotchkina, and V. Pervak, "Estimations of production yields for choosing of a practically optimal optical coating design," Appl. Opt. **50**, C141–C147 (2011).
11. T. V. Amotchkina, M. K. Trubetskov, V. Pervak, and A. V. Tikhonravov, "Design, production and reverse engineering of two-octave antireflection coatings," Appl. Opt. **50**, 6468–6475 (2011).
12. B. Badoil, F. Lemarchand, M. Cathelinaud, and M. Lequime, "Interest of broadband optical monitoring for thin-film filter manufacturing," Appl. Opt. **46**, 4294–4303 (2007).
13. B. Vidal, A. Fornier, and E. Pelletier, "Optical monitoring of nonquarterwave multilayer filters," Appl. Opt. **17**, 1038–1047 (1978).
14. A. V. Tikhonravov, M. K. Trubetskov, and T. V. Amotchkina, "Investigation of the effect of accumulation of thickness errors in optical coating production using broadband optical monitoring," Appl. Opt. **45**, 7026–7034 (2006).
15. A. V. Tikhonravov, M. K. Trubetskov, and T. V. Amotchkina, "On the reliability of computational estimations used for choosing the most manufacturable design," in *Optical Interference Coatings*, Technical Digest (CD) (Optical Society of America, 2011), paper TuA3.
16. A. V. Tikhonravov, M. K. Trubetskov, and T. V. Amotchkina, "Computational manufacturing experiments for choosing optimal design and monitoring strategy," in *Optical Interference Coatings*, Technical Digest (CD) (Optical Society of America, 2011), paper TuA5.
17. K. Friedrich, S. Wilbrandt, O. Stenzel, N. Kaiser, and K. Hoffmann, "Computational manufacturing of optical interference coatings: method, simulation results, and comparison with experiment," Appl. Opt. **49**, 3150–3162 (2010).
18. D. Ristau, H. Ehlers, S. Schlichting, and M. Lappschies, "State of art in deterministic production of optical thin films," Proc. SPIE **7101**, 71010C (2008).
19. M. Tilsch, K. Hendrix, and P. Verly, "Optical interference coating design contest 2004," Appl. Opt. **45**, 1544–1554 (2006).
20. H. Ehlers, S. Schlichting, C. Schmitz, and D. Ristau, "Hybrid process control for precision optics enhanced by computational manufacturing," in *Optical Interference Coatings*, Technical Digest (CD) (Optical Society of America, 2011), paper TuC6.
21. O. Stenzel, S. Wilbrandt, and N. Kaiser, "All-oxide broadband antireflection coatings by plasma ion assisted deposition: design, simulation, manufacturing and re-optimization," Opt. Express **18**, 8704–8708 (2010).
22. A. V. Tikhonravov and M. K. Trubetskov, "Computational manufacturing as a bridge between design and production," Appl. Opt. **44**, 6877–6884 (2005).
23. A. V. Tikhonravov and M. K. Trubetskov, OptiLayer Thin Film Software, http://www.optilayer.com.
24. D. Ristau, H. Ehlers, T. Gross, and M. Lappschies, "Optical broadband monitoring of conventional and ion processes," Appl. Opt. **45**, 1495–1501 (2006).
25. O. Stenzel, S. Wilbrandt, D. Fasold, and N. Kaiser, "A hybrid in situ monitoring strategy for optical coating deposition: application to the preparation of chirped dielectric mirrors," J. Opt. A **10**, 085305 (2008).
26. A. Zoeller, M. Boos, H. Hagedorn, and B. Romanov, "Computer simulation of coating processes with monochromatic monitoring," Proc. SPIE **7101**, 71010G (2008).
27. T. V. Amotchkina, S. Schlichting, H. Ehlers, M. K. Trubetskov, A. V. Tikhonravov, and D. Ristau, "Computational manufacturing as a key element in design-production chain for modern multilayer coatings," Appl. Opt. **51**, 7604–7615 (2012).
28. A. V. Tikhonravov, M. K. Trubetskov, and T. V. Amotchkina, "Investigation of the error self-compensation effect associated with broadband optical monitoring," Appl. Opt. **50**, C111–C116 (2011).
29. S. Furman and A. V. Tikhonravov, *Basics of Optics of Multilayer Systems* (Edition Frontieres, 1992).
30. S. Wilbrandt, O. Stenzel, N. Kaiser, M. K. Trubetskov, and A. V. Tikhonravov, "In situ optical characterization and re-engineering of interference coatings," Appl. Opt. **47**, C49–C54 (2008).
31. H. Macleod, "Monitoring of optical coatings," Appl. Opt. **20**, 82–89 (1981).
32. B. T. Sullivan and J. A. Dobrowolski, "Deposition error compensation for optical multilayer coatings. I. Theoretical description," Appl. Opt. **31**, 3821–3835 (1992).
33. A. V. Tikhonravov, M. K. Trubetskov, T. V. Amotchkina, G. DeBell, V. Pervak, A. K. Sytchkova, M. L. Grilli, and D. Ristau, "Optical parameters of oxide films typically used in optical coating production," Appl. Opt. **50**, C75–C85 (2011).

34. A. V. Tikhonravov, T. V. Amotchkina, M. K. Trubetskov, R. Francis, V. Janicki, J. Sancho-Parramon, H. Zorc, and V. Pervak, "Optical characterization and reverse engineering based on multiangle spectroscopy," Appl. Opt. **51**, 245–254 (2012).
35. T. V. Amotchkina, M. K. Trubetskov, V. Pervak, S. Schlichting, H. Ehlers, D. Ristau, and A. V. Tikhonravov, "Comparison of algorithms used for optical characterization of multilayer optical coatings," Appl. Opt. **50**, 3389–3395 (2011).
36. A. V. Tikhonravov and M. K. Trubetskov, "On-line characterization and reoptimization of optical coatings," Proc. SPIE **5250**, 406–413 (2004).